PHYSICAL REVIEW B **78**, 125301 (2008)

Influence of residual disorder on the anticrossing of Bloch modes probed in *k* space

N. Le Thomas, V. Zabelin, and R. Houdré
Institut de Photonique et d'Electronique Quantique, Ecole Polytechnique Fédérale de Lausanne (EPFL), Station 3, CH-1015 Lausanne, Switzerland

M. V. Kotlyar and T. F. Krauss
SUPA, School of Physics and Astronomy, University of St. Andrews, St. Andrews, Fife KY16 9SS, United Kingdom
(Received 26 May 2008; revised manuscript received 22 July 2008; published 2 September 2008)

We retrieve the dispersion properties of photonic crystal waveguides near the band edge with high experimental accuracy. The dispersion diagram of the waveguide modes in the complex-valued plane is directly measured in the far field by using a Fourier space imaging technique. We show that the investigation of the modes in *k* space provides a clear signature of the transition between propagating, evanescent, and localized modes. It allows us to determine the impact of the structural disorder and of the dissipation on the group velocity of the propagating wave in the slow light regime.

DOI: 10.1103/PhysRevB.78.125301 PACS number(s): 42.70.Qs, 72.15.Rn, 42.30.Kq, 42.25.Dd

I. INTRODUCTION

The propagation properties of quantum or classical waves are of fundamental interest. Since the investigations of waves propagating in a periodic medium by Lord Rayleigh in 1887,[1] the topic has played a crucial role in a large number of fields such as solid-state physics,[2] acoustic physics,[3] semiconductor superlattices,[4] integrated optics,[5] and photonic lattices.[6] One of the basic properties associated with periodic structures is the existence of frequency band gaps, which are widely used to engineer the propagation of waves. Such band gaps occur when the wave vectors of two modes and the reciprocal vector $\vec{G}$ of the periodic structure satisfy the Bragg condition.[2] Within the band gaps, the modes have complex-valued wave vectors and are evanescent whereas out with band gaps, the modes ideally propagate with purely real-valued wave vectors.

The presence of disorder can drastically affect the wave propagation and even lead to the Anderson localization, which was investigated, for instance, recently in photonic lattice[7] by controlling the amount of transverse disorder. As a positive consequence of the disorder in Bragg structures, band edges in photonic crystals were envisaged to promote and observe the transition toward Anderson localization of electromagnetic waves in three-dimensional (3D) structures,[8,9] which was traditionally investigated in random media such as GaAs powders.[10]

Alternatively, Bragg resonances are also the cornerstone for the realization of one-dimensional (1D) integrated nanophotonic structures with slow light propagation.[11,12] In such structures, disorder is undesirable and strongly impacts on the light propagation not only as a source of extrinsic losses[13] but also as catalyst of localization especially in the slow light regime. This apparent antagonism between the use of Bragg resonances for localization or slow light transport requires the determination of the transition region between the propagating and the localization regimes.

The theoretical impact of disorder on the wave transport in 1D system has been intensively investigated with the conclusion that an infinitesimal disorder is sufficient to localize the eigenstates.[14,15] To describe the transport close to a Bragg condition in ideal 1D photonic periodic structures, the two main analytical theories, i.e., the Floquet-Bloch (FB) (Refs. 16 and 17) and the coupled-mode (CM) theories,[18] focus on the dispersion curves $\omega(k)$. The dispersion curve, which describes the frequency ω of the wave as a function of its wave vector k, provides a clear insight into all essential propagation phenomena in photonic structures. Recent theoretical studies on photonic waveguides[19,20] have demonstrated that the presence of nanometer scale disorder drastically modifies the ideal dispersion near a band edge.

In contrast to the theoretical progress, no direct and complete (i.e., complex valued) experimental determination of the 1D dispersion curve $\omega(k)$ of periodic integrated dielectric structures near a stop band, identifying the role of the structural disorder, has been reported. The dispersion relation at frequencies in the vicinity of a band gap was measured in singly periodic planar waveguide via a prism coupler[21,22] in a photonic crystal structure loaded with quantum dots[23] and recently in a passive photonic crystal waveguide with phase-sensitive scanning near-field optical microscopy.[24] Such studies focused mainly on the real part of the wave vector and did not reveal the role played by the disorder. In addition, in all cases no clear evidence of the transition between propagating, localized, and evanescent modes was reported. Although some effects of the disorder on the wave transport can be inferred from the transmission of the medium[25–28] or from speckle pattern analysis,[29] we show that the determination of the dispersion curve in *k* space provides a physical picture of the wave propagation inside a medium subject to residual disorder.

In this paper we report the measurement of the entire experimental dispersion diagram $\omega(k)$ of a periodic quasi-1D model system operating near a band gap. By entire we mean the dispersion of the real and imaginary parts of the wave vector inside the medium. In particular, we focus on the role of disorder and the transition from light propagation to localization. We show that the *k* space imaging unambiguously sets the upper bound of the group velocity of the wave propagating near a disordered band edge.

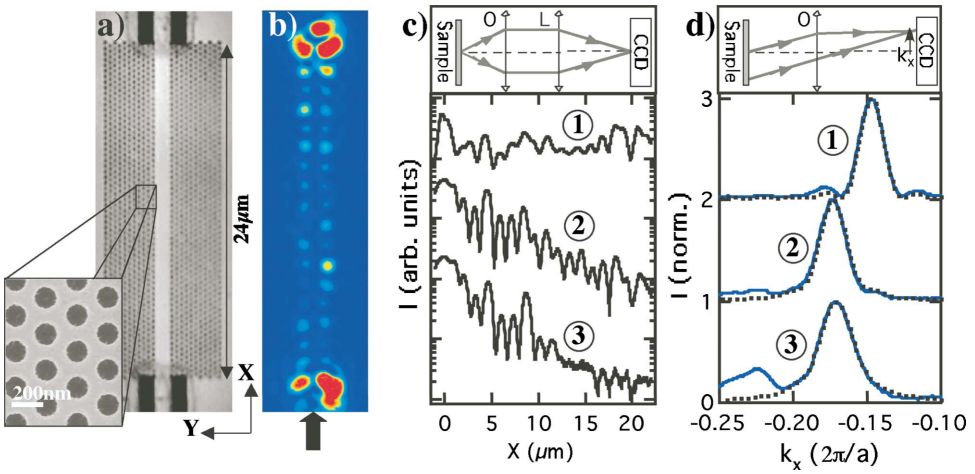

FIG. 1. (Color online) [(a) and (b)] Top view optical micrograph of the PhC waveguide and near infrared image of the propagating mode, respectively. Inset: Scanning electron microscope zoom of the PhC holes. [(c) and (d)] Intensity profile and angular spectrum of the field along the direction of propagation, respectively. Top: Schematics of the experimental setup used in both cases. O: microscope objective, L: imaging lens.

II. EXPERIMENTAL DISPERSION CURVES

Our model system, shown in Fig. 1(a), consists of a photonic crystal waveguide defined by three lines of missing holes along the ΓK direction in a two-dimensional (2D) triangular photonic lattice confining the light in the (x,y) plane. Such a structure, commonly called a W3 waveguide, can be considered as a periodic wire with the periodicity of the dielectric permittivity defined along the line defect by the air holes etched to form the 2D PhC lattice. The ministop band (MSB) arises from the anticrossing of the dispersion curves of two different Bloch modes coupled by the periodic modulation of the dielectric constant along the wire.[30]

To determine the intensity profile of a Bloch mode experimentally [Figs. 1(b) and 1(c)] as well as its dispersion curve (Fig. 2), we image its out-of-plane scattered components both in the standard real imaging space [see inset of Fig. 1(c)] and in the back focal plane of a high numerical aperture (NA=0.9) microscope objective [see inset of Fig. 1(d)]. The image in the back focal plane corresponds to the 2D spatial Fourier transform of the field radiated from the sample. It provides an accurate determination of the wave vectors of the different plane-wave components that constitute the Bloch modes propagating in the PhC, as recently demonstrated in Ref. 31. The wave vectors of the Bloch modes corresponding to spatial frequencies located inside the bandwidth of the imaging setup are directly and uniquely inferred.

To achieve a high modal selectivity, the modes are excited by a narrow bandwidth (0.001 nm) laser diode tunable from 1.48 to 1.66 μm range via standard lens fibers and access ridge waveguides [Fig. 1(a)]. The W3 waveguide (triangular lattice parameter $a=0.40$ μm, hole diameter $d=0.27$ μm, and total length $L=24$ μm) was designed to operate in the vicinity of the ministop band[30] for a TE polarized light around a wavelength of 1.55 μm. The GaInAsP/InP planar waveguide is single mode in the frequency range of interest with an effective index of 3.25. Details about the structural parameters and the fabrication are given in Ref. 31.

In Fig. 2, the experimental dispersion curves (colored curves) are compared and superimposed with the theoretical prediction (dark curves) calculated with a 2D plane-wave expansion (PWE) method.[32] The experimental plot is obtained by stacking together 200 normalized angular spectra, similar to the top spectrum, recorded in 0.5 nm wavelength steps and measured along the k_x direction of the PhC waveguide. The energy position of the zoomed angular spectra profiles in Fig. 1(d) is highlighted by labeled arrows. A very good agreement between the experimental and theoretical data is achieved in Fig. 2 provided that the dispersion of the refractive index of the constituting material of the InP planar waveguide is taken into account. Note that the wave vector of the forward propagating mode is negative, as already explained in Ref. 33. The band gap is located at $|k|\sim 0.17$ in units of $2\pi/a$ for normalized energies u ranging from 0.2592 to 0.2618. In principle, only forward propagating modes can be excited in ideal structures. Backward contributions are, however, measured for modes whose dispersion curve is flat, i.e., for low group velocity, such as the curve corresponding

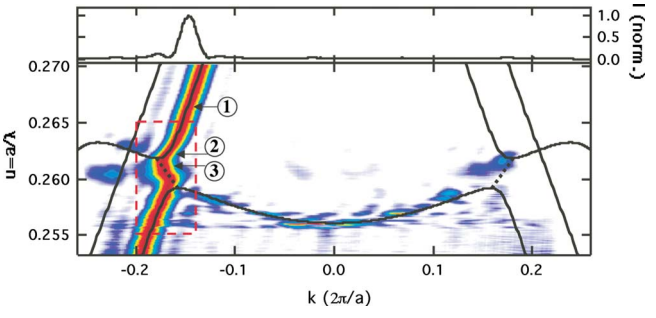

FIG. 2. (Color online) Theoretical (thin line) and experimental (2D color map) dispersion curves of a W3 PhC waveguide. The dashed rectangle locates the zooming region highlighted in Fig. 3. The labels 1, 2, and 3 correspond to the energy of the selected spectrum in Fig. 2. Top: normalized angular profile of the spectrum 1.

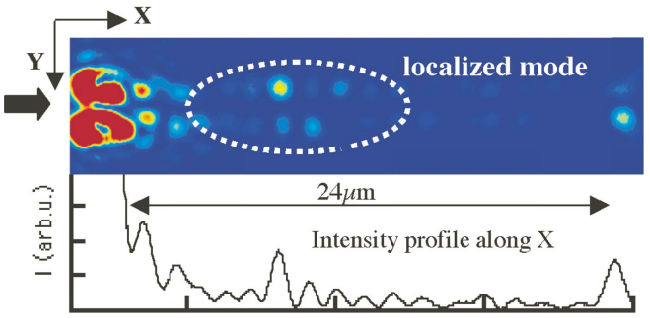

FIG. 3. (Color online) Imaging of a localized mode whose highest intensity is inside the W3 waveguide with $u=0.2596$.

to wave vectors k between −0.15 and 0.15. The contributions located at opposite k values and the discontinuities of the experimental dispersion curve of the slow mode located between $-0.1<k<0.1$ are an unambiguous signature of the presence of structural disorder. These observed scattered discontinuities correspond to localized states. In the following we concentrate on the band gap located inside the dashed red rectangle in order to estimate the disorder that produces these discontinuities in the dispersion diagram.

Figure 2 shows that radiated fields are also detected inside the band gap where light propagation is normally forbidden. These contributions come from the evanescent modes that remain localized at the waveguide input and have a finite imaginary wave vector component k_i. The real part of their wave vector k, calculated with PWE, is represented by a dotted line in Fig. 2 and is in agreement with the experimental values that are determined from the k-space positions of the Fourier spectra. Our near infrared (NIR) imaging microscope enables us to switch between the Fourier imaging space and the real imaging space [Fig. 1(b)].[31] As a result, the penetration length $l_c=1/(2k_i)$ can be simultaneously investigated in both the real and the Fourier spaces, as revealed by Figs. 1(d) and 1(c), respectively (note that in the Fourier space, the real and imaginary parts of the wave vector can be retrieved whereas in the real space, only the imaginary part is measured). In real space a decrease in l_c translates into an exponential decay of the profile of the envelope of the field with the largest damping in the middle of the band gap (spectrum 3). For propagating mode, i.e., outside of the band gap, the mode profile decay is negligible.

As expected from the Fourier transform of a decaying exponential function, the intensity of the angular spectrum [Fig. 1(c)] is well fitted with a Lorentzian function (dotted line in spectrum 3) as long as $l_c \ll L$. The convolution with a sinc function has to be considered when the sample size and l_c become comparable (spectrum 2). The transition from a Lorentzian line shape (no effect of the boundaries) to a "sinc" line shape (size effect) of the k-space spectrum is analogous to the phenomenological criteria of localization. According to this criterion, a wave function is considered localized if the eigenstate is not sensitive to the boundary condition.[34] In Fig. 3, the real-space imaging reveals the presence of modes fully localized inside the waveguide, i.e., modes that follow strictly the phenomenological criteria of localization. For a perfect sinc line shape (spectrum 1), which corresponds to the Fourier transform of a field constant over the entire sample, the mode can be considered as propagative. Note that the determination of the penetration length from the intensity decay profile in Fig. 1(c) is not accurate as the one retrieved from the linewidth of Fourier spectra due to interference processes between different modes. Nevertheless, the intrinsic modal selection in the Fourier space and the line-shape fitting procedure previously described provide a very accurate value of k_i, as plotted in Fig. 3(a).

III. RENORMALIZATION OF THE DISPERSION CURVES

Figure 4 is a magnification of the region of the ministop band. It highlights the departure of the experimental dispersion properties from an ideal 2D W3 waveguide. The nonideal behavior comes from the structural disorder and from the dissipation due to the intrinsic leaky nature of the quasiguided mode propagating in the planar structure, i.e., the intrinsic out-of-plane losses into the air and into the substrate. By highlighting the anticrossing between a "slow" mode, whose dispersion curve is relatively flat, and a "fast" mode, our goal is to give an upper quantitative limit of the structural disorder through its impact on the ideal band gap. In addition to the dispersion curves of the real k and imaginary k_i parts of the wave vector [Fig. 4(a)], the transmission curve [Fig. 4(b)] and the dispersion of the group index n_g [Fig. 4(c)] allow us to unambiguously define the frequency regions of ideal behavior (gray band), and the regions of the renormalization of the dispersion curve due to disorder and dissipation (white band). In the gray regions, the experimental dispersion of k and k_i as well as the dispersion of the group index follow, with high precision, the PWE calculation of the ideal structure. The departure from the ideal case (white band) takes place either for large group indices ($0.26181<u<0.2623$ and $0.2584<u<0.2592$), which are revealed by an abrupt change of the curvature of the dispersion curve [highlighted by the group index $n_g=1/(du/dk)$] or for long penetration lengths (i.e., small k_i) of the evanescent modes inside the band gap. In both cases, the impact of disorder and dissipation can be correlated with the interaction time of the field within the sample: a slow group velocity for propagating modes (outer white domain) and a long penetration length for evanescent modes (inner white domain) imply a long interaction time with the disorder and the pure dissipation.

IV. ONE-DIMENSIONAL MODELING OF THE DISORDER AND OF THE DISSIPATION

In Fig. 4(c) we show that the disorder and the pure dissipation have a drastic impact on the group index, i.e., on the group velocity of the propagating wave. The theoretical divergence of the group index, which implies ultraslow light, is destroyed due to the renormalization of the energy u in the presence of disorder. As a result, the group index does not exceed ten. Note that the group index is not a well defined quantity in a 1D disordered structure due to the statistical nature of the problem. The density of states, which is pro-

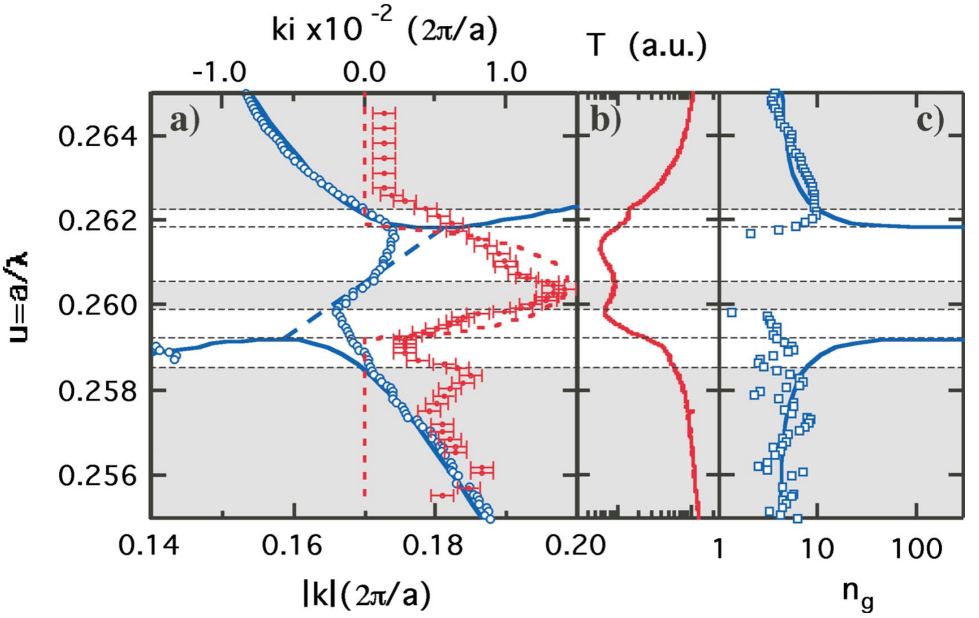

FIG. 4. (Color online) (a) Zoom of the experimental (open circle) and theoretical (blue line) dispersion curves near the stop band of the PhC waveguide. The imaginary part of the wave vector inside the band gap is represented with plain red points for the experimental data and small dash line for the theory (upper scale). (b) Transmission of the waveguide (log scale). (c) Theoretical and experimental group indices.

portional to the group index for an ideal 1D structure, is a more appropriate physical quantity. Nevertheless, in the current case, the linewidths of the far-field spectra are broader than the k-space distribution induced by the disorder near the anticrossing region. As a result, we define the group index from the dispersion curve of the position of the maxima of the k-space spectra. The saturation effect of the 1D density of states due to disorder is well known,[35] and can be calculated for instance by using the effective-medium model and the coherent-potential approximation (CPA).[36] However this calculation does not take into account the dissipation such as intrinsic out-of-plane losses. We develop here a simple 1D transfer quasiperiodic matrix model involving the effective indices of the modes of the 2D system to estimate quantitatively the amount of disorder as well as of dissipation. This model allows us to directly reproduce the experimental dispersion curves. We use a similar approach as the one used in Ref. 37: We consider a linear chain of N cells of length a with a modal propagation inside the cells, and transmission and reflection at each junctions of the cells, as illustrated in Fig. 5(a). The complex amplitudes m_1 and m_2 of two contrapropagating modes with index n_1 and n_2, respectively, are then related by a transfer matrix A_n between cell n and $n+1$, which can be expressed as

$$\begin{pmatrix} m_1 \\ m_2 \end{pmatrix}_{n+1} = A_n \begin{pmatrix} m_1 \\ m_2 \end{pmatrix}_n, \tag{1}$$

$$A_n = \begin{pmatrix} e^{-i(2\pi/\lambda_0)an_1} & 0 \\ 0 & e^{i(2\pi/\lambda_0)an_2} \end{pmatrix} \begin{pmatrix} 1/T_n^* & -(R_n/T_n)^* \\ -R_n/T_n & 1/T_n \end{pmatrix}, \tag{2}$$

with T_n and R_n as the appropriate complex transmission and reflection coefficients. For a periodic and an infinite structure, it can be shown by applying Bloch's theorem that the eigenvalues λ of A_n have the form $\lambda=\exp(ik_e a)=\exp(ika-k_i a)$. As a result, the dispersion curves ω versus k are determined from the phase of these eigenvalues. By choosing the proper values of the input parameters: the indices n_1 and n_2, the modulus $|T_n|$, and the phase ϕ_T of the transmission coefficient, we show in Fig. 5(b) that the 1D transfer-matrix model reproduces perfectly the 2D PWE calculation. For instance, for the filling factor $f=0.31$, a very good fit is obtained with $n_1=19.9694$ (slow mode), $n_2=3.3131$ (fast mode), $|T_n|=0.9955$, and $\phi_T=0.065\pi$ in all the cells. The reflection coefficient is given by $R_n=\sqrt{1-|T_n|^2}$, which corresponds to undamped junctions. In contrast to 2D PWE calculation, in the framework of such a 1D model, the effects of the disorder and of the pure dissipation can be determined separately and analytically. We first discuss the influence of the disorder.

The continuous shape of the experimental dispersion curves near the anticrossing suggests that the disorder is sufficiently small to treat the chain as a quasiperiodic system. In addition, with the hypothesis of a random variation of the structural disorder that is considered statistically independent and homogeneous in each cells, the ensemble-average behavior of the system is determined by the average transfer matrix over all the realization of the disorder. The system is then modeled by a periodic chain with the same averaged transfer matrix $\bar{A}$ between each cell. As in the ideal case, the calculation of the eigenvalues of $\bar{A}$ gives a direct access to the dispersion curves in presence of "small" structural disorder.

The random variable that we consider is the radius r of the holes with a Gaussian distribution $p(r)$ whereas the lattice parameter a is kept constant. The calculation is similar in the case of the fluctuation of the position of the hole. All the

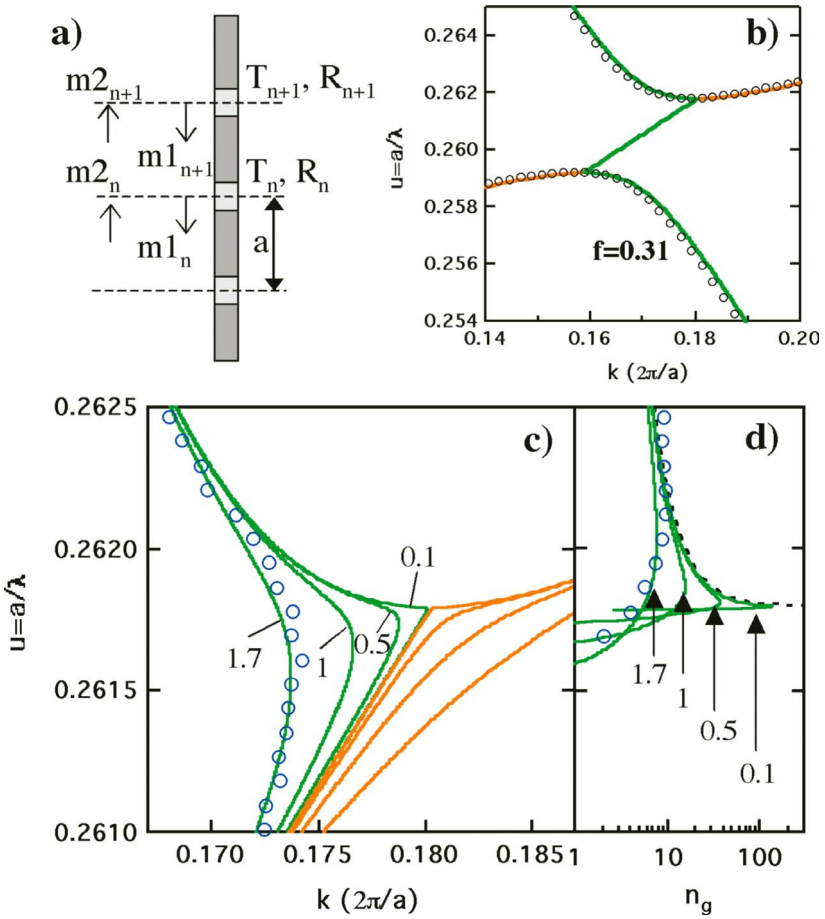

FIG. 5. (Color online) (a) Schematic of the modeled 1D chain (see text). (b) 2D plane-wave expansion (circles) and 1D transfer-matrix (lines) calculations of the W3 dispersion curves for $f=0.31$. (c) Theoretical renormalization of the dispersion curves of the fast mode (green color) and slow mode (orange color) near the upper band edge for different standard deviations of the hole size σ_r (label in nanometers). (d) Corresponding group index of the fast mode for the same σ_r. The open circles are the experimental data.

coefficients of the transfer matrix in presence of the disorder are given by $\bar{A}_{ij}=\int A_{ij}p(r)dr$. Their calculation requires investigating the input parameters of the 1D transfer-matrix model that are influenced by the distribution of the size of the holes.

A fluctuation of the radius r of the holes induces a concomitant fluctuation of the filling factor f. From the 2D PWE calculation, we determine the corresponding variation of the fitting parameters of the 1D model. A positive variation of the indices produces a horizontal rigid shift of the dispersion curves toward larger k whereas a positive variation of the phase of the transmission coefficient produces an oblique rigid shift toward the decreasing k vectors. As a result of the fitting procedure, the input parameters of the 1D model possess a linear dependence versus the radius, and their variations are given by $\frac{\Delta n_1}{\Delta r}=\frac{\Delta n_2}{\Delta r}\approx 13\frac{f_0}{r_0}$ and $\frac{\Delta \Phi_T}{\Delta r}\approx 18\pi\frac{f_0}{r_0}$. It follows that the average transfer matrix can be written as

$$\bar{A}=\begin{bmatrix} 1/T^{*}e^{-i2\pi un_1-(1/2)\sigma_r^2[2\pi u(\Delta n_1/\Delta r)-(\Delta\Phi_T/\Delta r)]^2} & -(R/T)^{*}e^{-i2\pi un_1-(1/2)\sigma_r^2[2\pi u(\Delta n_1/\Delta r)-(\Delta\Phi_T/\Delta r)]^2} \\ -(R/T)e^{i2\pi un_2-(1/2)\sigma_r^2[2\pi u(\Delta n_2/\Delta r)+(\Delta\Phi_T/\Delta r)]^2} & 1/Te^{i2\pi un_2-(1/2)\sigma_r^2[2\pi u(\Delta n_2/\Delta r)+(\Delta\Phi_T/\Delta r)]^2} \end{bmatrix}, \quad (3)$$

where σ_r is the standard deviation of the Gaussian radius distribution. The dispersion curves obtained with such an averaged transfer matrix are shown in Fig. 5(c) near the upper band edge for different σ_r, as well as the corresponding group index in Fig. 5(d). When σ_r reaches 1.7 nm, the model reproduces well the experimental data, which settles an upper limit for the disorder related to the fluctuation of the size of the holes. This simple calculation shows that a radius

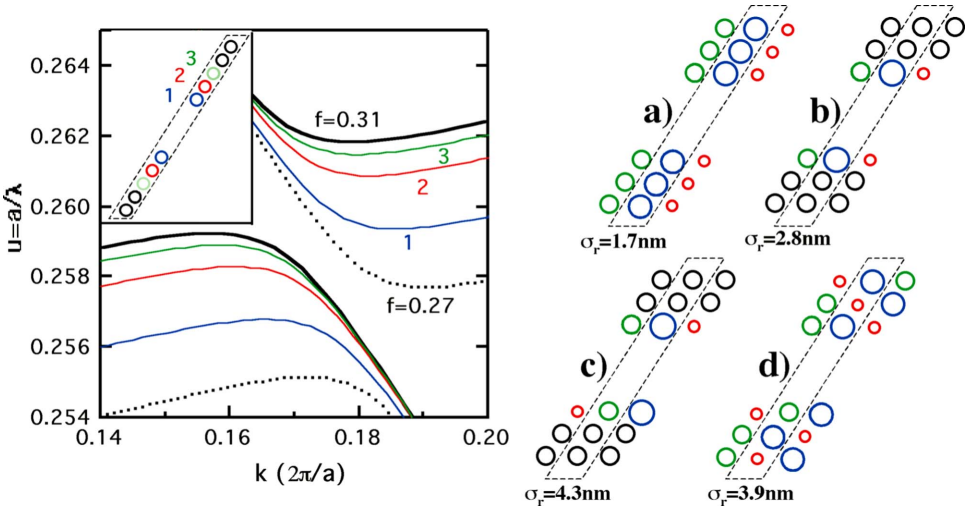

FIG. 6. (Color online) Left: Variation of the theoretical W3 anticrossing of the dispersion curves for a decrease in the filling factor down to 0.27 for the first (case 1), second (case 2), or third (case 3) lines of holes, separately, as labeled in the inset, with the filling factor of all the unchanged lines of holes equal to 0.31. The dark continuous and dotted lines correspond to bulk filling factor of 0.31 and 0.27, respectively. Right: Schematic representation of different disorder configurations with the corresponding standard deviation σ_r of the radius distribution that fits the experimental data; (a) Identical fluctuation of the size of the holes in a given elementary supercell (dotted trapeze), (b) correlated disorder of the two first symmetric lines of holes with the other holes unperturbed, (c) uncorrelated fluctuations of the two first symmetric lines of holes with the other holes unperturbed, and (d) random disorder in all the structure.

fluctuation of only 1.7 nm already limits the group index to eight. Note that for σ_r as low as 0.1 nm, which constitutes a challenging technological limit, the maximum of the group index is still limited to only 150.

Until now we have considered a global fluctuation of the radius of all the holes in the same elementary supercell [case (a) in Fig. 6]. Figure 6 shows that the transverse disorder, i.e., the disorder inside a given elementary supercell, can be taken into account within our simple 1D model. The variation induced by a fluctuation of the size of the hole depends on the position of the hole in the supercell. The variation of the size of the holes that border the W3 defect induces the largest rigid shift of the anticrossing, which is not surprising considering that the transverse profile of the guided mode extend only over a couple of holes. If we take into account the size fluctuation of only the two symmetric first lines of holes [case (b)], the standard deviation σ_r that fits the experimental data is 2.8 nm. In this case, the holes located on each sides of the W3 defect are still correlated. However, it is possible in a linear approximation to treat the uncorrelated case if independent random variables are associated to each line of holes. For instance, if only two independent lines of holes are considered, the terms $(2\pi u\frac{\Delta n_i}{\Delta r} \pm \frac{\Delta \Phi_T}{\Delta r})^2$ in the average matrix $\bar{A}$ are replaced by $\{[2\pi u(\frac{\Delta n_i}{\Delta r})_p \pm (\frac{\Delta \Phi_T}{\Delta r})_p]^2 + [2\pi u(\frac{\Delta n_i}{\Delta r})_q \pm (\frac{\Delta \Phi_T}{\Delta r})_q]^2\}$, with $i=1,2$, and where the indices p and q differentiate between the lines of holes. In the case of the uncorrelated two first lines of holes [case (c)], the input parameters of the 1D model that results from the 2D PWE calculation are $\{\frac{\Delta n_i}{\Delta r}\}_p = \{\frac{\Delta n_i}{\Delta r}\}_q \approx 3.7\frac{f_0}{r_0}$ and $\{\frac{\Delta \Phi_T}{\Delta r}\}_p = \{\frac{\Delta \Phi_T}{\Delta r}\}_q \approx 2.25\pi\frac{f_0}{r_0}$. It follows that the standard deviation σ_r that fits the experimental data is 4.3 nm. When all the lines of holes of the PhC are uncorrelated [case (d)] with random Gaussian distributions, we find $\sigma_r = 3.9$ nm. As a result, the correlation in the transverse direction [case (a)] overestimates the effect of the disorder compared to the uncorrelated one [case (d)].

Note that in general a 1D model can only treat the disorder in the longitudinal direction (i.e., the propagating direction). Here, the incorporation of the disorder in the transverse direction relies on the use of the 2D PWE, which provides the input parameters of the 1D model, as well as on the approximation of independent random variables for each holes. Moreover, we have used a linear approximation of the input parameter $\frac{\Delta n_i}{\Delta r}$ and $\frac{\Delta \Phi_T}{\Delta r}$ in order to add the independent contributions of all the holes. Such an approximation is satisfied for the small fluctuation range considered here according to the 2D PWE calculation.

The effect of the dissipation, which constitutes the second source of renormalization, is directly incorporated in the transfer matrix of the ideal structure as a damping factor during the propagation inside the cells: The terms $e^{-i(2\pi/\lambda_0)an_1}$ and $e^{i(2\pi/\lambda_0)an_2}$ are replaced by $e^{-i(2\pi/\lambda_0)an_1-\alpha_1}$ and $e^{i(2\pi/\lambda_0)an_2-\alpha_2}$ with α_1 and α_2 as the propagation losses of the slow and fast modes, respectively. The ratio of the fast mode and slow mode losses is given by $\alpha_1/\alpha_2 = \gamma(n_1/n_2)$, where the coefficient $\gamma=7$ takes into account the difference of the overlap between the field map and the hole map for the two modes. For fast mode losses of 33 cm^{-1}, the calculated dispersion curve (without disorder) is identical to the dispersion curves obtained in the case of a pure hole size fluctuation with $\sigma_r = 1.7$ nm. Such a value is in agreement with the ones obtained from internal light source measurement.[38] This 1D model allows us also to settle a maximum value for the out-of plane losses.

It is not surprising within the hypothesis of the current model that the calculated dispersion curves have the same shape in presence of small structural disorder or with out-of

plane losses as both cases represent a damping process that affect the investigated mode. The structural disorder mainly redistributes the energy among modes that belong to the "closed" system, in contrast to the out-of plane losses. As the Fourier space imaging technique provides a modal analysis, probing the imaginary part of the wave vector gives a direct access to such an energy transfer between the modes of the structure. This is particularly highlighted in Fig. 2 for $u < 0.258$ where k_i undergoes strong fluctuations whereas the transmission is similar to the region $u > 0.263$ where k_i is almost unaffected by the disorder. For the current sample length L, which is of the order of magnitude of $1/(2k_i)$, the transmission is not affected by the modal redistribution induced by the disorder as it cannot discriminate the contributions of the different states excited in the system.

V. CONCLUSION

In conclusion, we have measured the dispersion curve near the stop band of a 1D periodic waveguide in the k space. This experimental technique allows us to accurately determine the band edges, i.e., the onset of forbidden guided wave propagation, in real structures under real condition of operation. Based on a simple 1D transfer matrix, the W3 waveguide constitutes a model system to investigate the impact of the structural disorder induced by the fabrication on the fundamental optical properties of the PhC devices. The present study can in principle be extended to Bloch modes with spatial harmonics located below the light line with the use of linear probe gratings,[39] which offer control on the dissipation. The imaging in Fourier space that gives access to the imaginary part of the dielectric permittivity is also of prime importance for the investigation of gain materials (represented by the imaginary part of the dielectric permittivity) such as bulk, quantum well, quantum wire, and quantum dots, and/or to investigate dispersion effects in optical amplifiers structures operating in the slow light regime. Finally, our approach, which also provides the renormalization of the 2D equifrequency surfaces of PhCs,[31] is particularly appealing for detecting the presence of a photon mobility edge in 2D structures, as recently numerically predicted in Ref. 40.

ACKNOWLEDGMENTS

This project was supported by the European network of excellence ePIXnet Contract No. IST-004525, Funfox Contract No. IST-004582, the Swiss Quantum Photonics National Center for Competence in Research, and the COST action P11. We would like to thank Hua Zhang for the SEM image of the PhC structure and Vincenzo Savona for helpful discussions.

[1] Lord Rayleigh, Philos. Mag. **24**, 145 (1887).
[2] C. Kittel, *Introduction to Solid State Physics* (Wiley, New York, 1967).
[3] D. M. Profunser, O. B. Wright, and O. Matsuda, Phys. Rev. Lett. **97**, 055502 (2006).
[4] R. Dingle, A. C. Gossard, and W. Wiegmann, Phys. Rev. Lett. **34**, 1327 (1975).
[5] C. Elachi and C. Yeh, J. Appl. Phys. **44**, 3146 (1973).
[6] G. Bartal, O. Cohen, H. Buljan, J. W. Fleischer, O. Manela, and M. Segev, Phys. Rev. Lett. **94**, 163902 (2005).
[7] T. Schwartz, G. Bartal, S. Fishman, and M. Segev, Nature (London) **446**, 52 (2007).
[8] S. John, Phys. Rev. Lett. **58**, 2486 (1987); Comments Condens. Matter Phys. **14**, 193 (1988).
[9] V. Yannopapas, A. Modinos, and N. Stefanou, Phys. Rev. B **68**, 193205 (2003).
[10] D. S. Wiersma, P. Bartolini, A. Lagendijk, and R. Righini, Nature (London) **390**, 671673 (1997).
[11] M. Notomi, K. Yamada, A. Shinya, J. Takahashi, C. Takahashi, and I. Yokohama, Phys. Rev. Lett. **87**, 253902 (2001).
[12] Y. A. Vlasov, M. OBoyle, H. F. Hamann, and S. J. NcNab, Nature (London) **438**, 65 (2005).
[13] S. Hughes, L. Ramunno, J. F. Young, and J. E. Sipe, Phys. Rev. Lett. **94**, 033903 (2005).
[14] B. Kramer and A. MacKinnon, Rep. Prog. Phys. **56**, 1469 (1993).
[15] P. Sheng, *Introduction to Wave Scattering, Localization, and Mesoscopic Phenomena* (Academic, Boston, 1995).
[16] T. Tamir, H. C. Wang, and A. A. Oliner, IEEE Trans. Microwave Theory Tech. **12**, 323 (1964).
[17] P. St. J. Russell, Appl. Phys. B **39**, 231 (1986).
[18] D. Marcuse, Bell Syst. Tech. J. **48**, 3187 (1969).
[19] S. Mookherjea and A. Oh, Opt. Lett. **32**, 289 (2007).
[20] M. A. Kaliteevski, D. M. Beggs, S. Brand, R. A. Abram, and V. V. Nikolaev, Phys. Rev. B **73**, 033106 (2006).
[21] R. Zengerle, J. Mod. Opt. **34**, 1589 (1987).
[22] M. Galli, D. Bajoni, M. Patrini, G. Guizzetti, D. Gerace, L. C. Andreani, M. Belotti, and Y. Chen, Phys. Rev. B **72**, 125322 (2005).
[23] D. Labilloy, H. Benisty, C. Weisbuch, C. J. M. Smith, T. F. Krauss, R. Houdré, and U. Oesterle, Phys. Rev. B **59**, 1649 (1999).
[24] H. Gersen, T. J. Karle, R. J. P. Engelen, W. Bogaerts, J. P. Korterik, N. F. van Hulst, T. F. Krauss, and L. Kuipers, Phys. Rev. Lett. **94**, 073903 (2005).
[25] L. Braginsky and V. Shklover, Phys. Rev. B **73**, 085107 (2006).
[26] B. M. Möller, U. Woggon, and M. V. Artemyev, Phys. Rev. B **75**, 245327 (2007).
[27] D. Nau, A. Schönhardt, Ch. Bauer, A. Christ, T. Zentgraf, J. Kuhl, M. W. Klein, and H. Giessen, Phys. Rev. Lett. **98**, 133902 (2007).
[28] J. Topolancik, B. Ilic, and F. Vollmer, Phys. Rev. Lett. **99**, 253901 (2007).
[29] V. M. Apalkov, M. E. Raikh, and B. Shapiro, Phys. Rev. Lett. **92**, 253902 (2004).
[30] S. Olivier, M. Rattier, H. Benisty, C. Weisbuch, C. J. M. Smith, R. M. De La Rue, T. F. Krauss, U. Oesterle, and R. Houdré, Phys. Rev. B **63**, 113311 (2001).

[31] N. Le Thomas, R. Houdré, M. V. Kotlyar, D. OBrien, and T. F. Krauss, J. Opt. Soc. Am. B **24**, 2964 (2007).
[32] M. Plihal and A. A. Maradudin, Phys. Rev. B **44**, 8565 (1991).
[33] N. Le Thomas, R. Houdré, M. V. Kotlyar, and T. F. Krauss, Phys. Rev. B **77**, 245323 (2008).
[34] D. J. Thouless, Phys. Rev. Lett. **39**, 1167 (1977).
[35] I. M. Lifshits, S. A. Gredeskul, and L. A. Pastur, *Introduction to the Theory of Disordered Systems* (Wiley, New York, 1988).
[36] M. Lax, Rev. Mod. Phys. **23**, 287 (1951).
[37] R. S. Langley, J. Sound Vib. **188**, 717 (1995).
[38] S. Olivier, H. Benisty, C. Weisbuch, C. J. M. Smith, T. F. Krauss, and R. Houdré, Opt. Express **11**, 1490 (2003).
[39] N. Le Thomas, R. Houdré, L. H. Frandsen, J. Fage-Pedersen, A. V. Lavrinenko, and P. I. Borel, Phys. Rev. B **76**, 035103 (2007).
[40] A. A. Asatryan, L. C. Botten, M. A. Byrne, R. C. McPhedran, and C. M. de Sterke, Phys. Rev. E **75**, 015601(R) (2007).